Determination of winding destroy limit area for a power series of amorphous core transformers

Doan Thanh Bao*

Faculty of Engineering & Technology, Quy Nhon University, 170 An Duong Vuong, Quy Nhon, Binh Dinh, Vietnam.

*Corresponding author: doanthanhbao@qnu.edu.vn

Received 24 Feb. 2025; Revised 12 Apr. 2025; Accepted 09 May 2025; Published 25 May 2025.

DOI: https://doi.org/10.54939/1859-1043.j.mst.103.2025.11-21

ABSTRACT

The amorphous steel core transformer features a unique structure with a rectangular winding, resulting in an uneven distribution of electromagnetic force compared to the circular winding of silicon core transformers. Consequently, evaluating the added value of electromagnetic waves and identifying the destructive areas of winding are crucial. In this paper, the combination of Matlab and the finite element technique is developed to calculate the magnetic field, short-circuit current, and electromagnetic force for 3-phase amorphous transformers (22/0.4 kV) during short-circuit faults. The findings establish a relationship between the electromagnetic force value during a short circuit and the winding radius, as well as identify the areas where the winding damage is confined based on the transformer power sequence. These research results assist designers, manufacturers, and transformer operators in determining the appropriate harmful conditions of short-circuit electromagnetic force for the windings.

Keywords: Transformer; Amorphous; Electromagnetic force; Magnetic field; Short-circuit; Finite element method.

1. INTRODUCTION

When power systems use amorphous core transformers (APCTs), they experience lower operating costs and reduced losses compared to traditional silicon steel core transformers. APCTs enhance economic efficiency significantly by cutting no-load losses by 60–70% [1]. Due to the unique structure of the amorphous steel core and its rectangular windings, the distribution of the electric field, magnetic field and electromagnetic forces (EMFs) is asymmetrical along the winding turns. The bending points of the windings are particularly vulnerable, as they have the lowest mechanical strength under EMFs. During normal operation, the EMFs induce vibrations and noise in the APCTs. Under the combined influence of EMFs and Lorentz forces, transformer windings may experience deformation and displacement [2-4]. In the event of a short circuit, the resulting high EMFs can be extremely dangerous, leading to wire displacement, bending, or even breakage at the winding bend angles [5-8]. In [9], the study analyzed the magnetic field of the transformer when a short circuit occurs. In this paper, the author combined analytical calculations with numerical simulations to investigate the transformer under both normal and short-circuit conditions. The axial and radial forces obtained from these two approaches were then compared and evaluated. In [10, 11], the paper also analyzed and calculated the short-circuit EMFs of a silicon steel core transformer with a circular cross-section using the FEM. The authors confirmed that when the transformer is short-circuited while operating in the power system, the short-circuit currents interact with the stray magnetic flux, causing severe mechanical stress on the transformer winding. The authors examined the radial force on the low voltage (LV) winding at 16 different locations. In [12, 13], the results of the force distribution values on the 16 points were relatively uniform. The distributions of the scattered magnetic fields, dissipative reactance and EMFs affecting the high voltage and LV windings of the transformer in case of short-circuit are simulated by the FEM. In [14], the paper investigated EMFs and mechanical stresses in transformers, highlighting their critical role in transformer operation and stability. Proper evaluation of these forces is essential for optimizing

transformer design. The paper proposed a method for optimizing EMFs in transformers with multiple sections on the HV winding. The impact of section count on EMFs in dry-type transformers was analyzed using three-dimensional finite element models. Additionally, in [15], authors presented an analysis of the electromagnetic and mechanical characteristics of a converter transformer under inrush current, emphasizing its importance in transformer performance and reliability. In [16], The simulation results revealed that radial forces have a greater impact on the winding than axial forces, with the intermediate phase (Phase B) experiencing the most significant effect. In [17], the Matlab/Simulink was applied for an 800 kVA dry-type transformer product to obtain the inrush current under different closing angles and residual magnetism effects. By applying the field-circuit coupling method, the obtained excitation inrush current from Simulink is imposed as an excitation on the transformer winding, resulting in EMFs acting on the winding. Finally, the electromagnetic-structural combined simulation is used to compare and study the deformation and forces on the transformer winding. In [18-20], the authors have used the FEM to analyze and calculate the distribution of dissipated magnetic field, dissipated reactance and EMFs acting on the HV and LV windings of the transformer in case of the short-circuit. The obtained results from FEM were then compared with the classical analysis method.

The above analysis reveals a lack of comprehensive evaluation of short-circuit conditions in transformers. A precise model is needed to accurately assess the maximum current interacting with the magnetic field. To address this, our paper presents a detailed analysis across various transformer capacities, evaluating short-circuit currents and the resulting EMFs. From these results, the characteristics of EMFs in relation to the winding radius and identify the transformer winding protection zone will be established. These findings are valuable for transformer manufacturers in optimizing winding design, for operators in determining appropriate short-circuit interruption times, and for selecting self-falling fuses to protect transformers from the destructive effects of short-circuit EMFs.

2. ANALYTIC MODEL FOR CALCULATING LEAKAGE MAGNETIC FIELDS

The Laplace-Poisson's equation for **A**(x,y,z) can be obtained based on the Maxwell's equations (where ($\partial/\partial t = 0$) as follows [7, 10, 12, 20]:

$$\nabla^2 \mathbf{A}(x, y, z) = \begin{cases} -\mu \mathbf{J} & \text{in the windings} \\ 0 & \text{others} \end{cases} \tag{1}$$

In three-dimensional Descartes coordinates, the magnetic field is perpendicular to the plane ($\partial A/\partial z = 0$). the equation (1) can be written as:

$$\frac{\partial^2 \mathbf{A}(x, y)}{\partial x^2} + \frac{\partial^2 \mathbf{A}(x, y)}{\partial y^2} = -\mu \mathbf{J} \tag{2}$$

where **A**(x,y,z) is the magnetic vector potential, μ is the relative permeability (H/m) and **J** is the electric current density in the windings (A/m^2).

The **A** (x,y) in the equation (2) can be analysed in the form of a harmonic series

$$\mathbf{A}(x, y) = \sum_j \sum_k A_{j,k} \cos(m_j x).\cos(n_k y) \tag{3}$$

The magnetic flux density (**B**) can be given as $\mathbf{B} = \nabla \times \mathbf{A}$, the components of **B** ($\mathbf{B}_x$ and $\mathbf{B}_y$) at the boundary conditions of the magnetic window can be expressed as:

$$\begin{cases} B_x = \dfrac{\partial \mathbf{A}(x, y)}{\partial y} \\ B_y = -\dfrac{\partial \mathbf{A}(x, y)}{\partial x} \end{cases} \tag{4}$$

The magnetic vector potential of **A** and the magnetic flux density of **B** in the LV and HV windings are analysed by FEM.

3. APPLICATION TEST

3.1. The parameters of power transformer 50 kVA-22/0,4 kV

The test problem is the practical problem of the APCTs of 50 kVA – 22/0.4 kV. The detailed parameters of the APCTs are given in table 1.

Table 1. *The fundamental specifications of the APCTs of 50 kVA – 22/0.4 kV.*

No.	Parameters	Value
1	The number of phases	3
2	Frequency (Hz)	50
3	Rated power (kVA)	50
4	Winding diagram	Δ/Y-11
5	Rated voltages HV/LV (kV)	22/0.4
6	Number of turns per phase in HV/LV (turns)	4002/40
7	Rated phase currents HV/LV (A)	0.76/72.17
8	No load current ratio (i_0%)	0.8
9	Short circuit voltage u_k (%)	4.2

The model of APCTs of 50 kVA is shown in figure 1 shows. The complete manufacturing process is pointed in figure 2.

Figure 1. *The model of APCTs of 50 kVA.*

Figure 2. *The production process of APCTs of 50 kVA.*

3.2. Short-circuit currents and leakage fields in LV and HV windings

The short-circuit current flowing in the windings has the potential to cause damage to the transformer windings. This transient short-circuit current comprises two different components, namely [9, 10, 18].

$$\begin{aligned} i_{SCC} &= i_{har} + i_{dam} \\ &= I_n\sqrt{2}.\sin\left(\omega t - \varphi_n\right) + I_n\sqrt{2}.\sin(\varphi_n).e^{-\frac{R_n}{X_n}\omega t} \end{aligned} \tag{5}$$

where the current i_{SCC} consists of two components, i.e., the alternating and sinusoidal component i_{har} and the aperiodic component i_{dam}. φ_n, R_n, and X_n are the phase angle of the short-circuit current, short-circuit resistance, and short-circuit reactance, respectively.

Based on the basic parameters of the transformer given in table 1, the transient currents in the LV and HV windings are respectively calculated as follows:

$$i_{nHV} = i_{har} + i_{dam} = 18.1\sqrt{2}\sin\left(100\pi t - 1.57°\right) + 18.1\sqrt{2}\sin 90.2^{0} e^{-\frac{114.5}{91.6}100\pi t} (A) \quad (6)$$

$$i_{nLV} = i_{har} + i_{dam} = 1718.33\sqrt{2}\sin\left(100\pi t - 1.57°\right) + 1718.33\sqrt{2}\sin 90.6^{0} e^{-\frac{114.5}{91.6}100\pi t} (A) \quad (7)$$

The transient currents in the equations (6) and (7) are pointed out in figure 3 and figure 4. It can be seen that the currents reach maximum values at the first peak of 4007.3 (A) for the LV winding and 41.15 (A) for the HV winding.

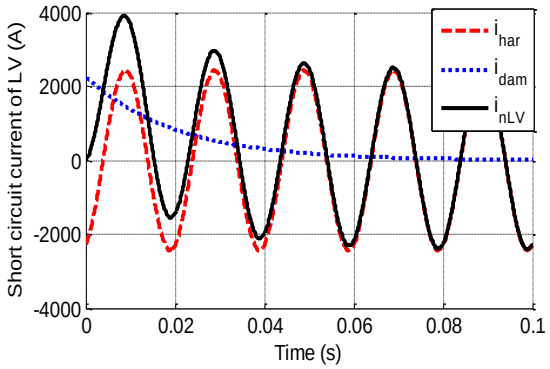

Figure 3. *Distribution of the short-circuit current in the LV winding.*

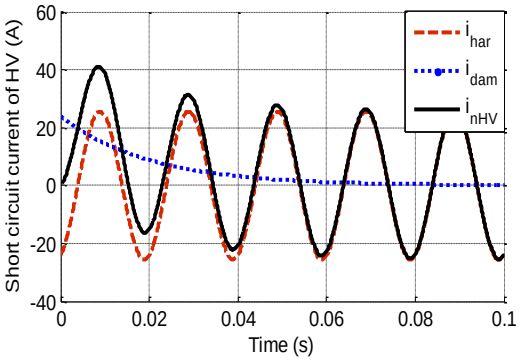

Figure 4. *Distribution of the short-circuit current in the HV winding.*

3.3. Finite element method

In this part, the FEM is developed to simulate electromagnetic parameters of the APCTs of 50 kVA-22/0,4 kV. The meshing model of the APCTs is given in figure 5, where tetrahedral elements were used. The APCTs model was meshed with a total of 871000 elements. In order to reduce the computer computation time and make the analysis more efficient, the insulation material and supporting structure are ignored in this model. Also, the concentric arrangement of windings is considered in the Maxwell 3D model. The analysis duration is set to 0.2 s, with a time step of 0.0001 s. This allows for detailed results on the magnetic inductance distribution within the magnetic circuit and windings throughout the entire operating period of the APCTs, as shown in figure 6.

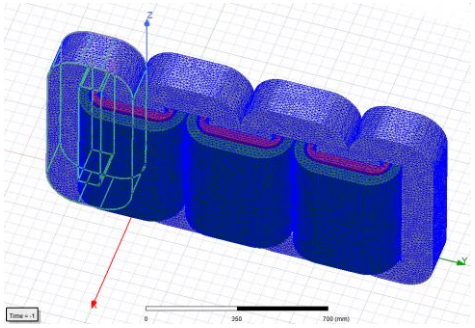

Figure 5. *Mesh plots of the 50 kVA APCTs generated in Ansys Maxwell 3D.*

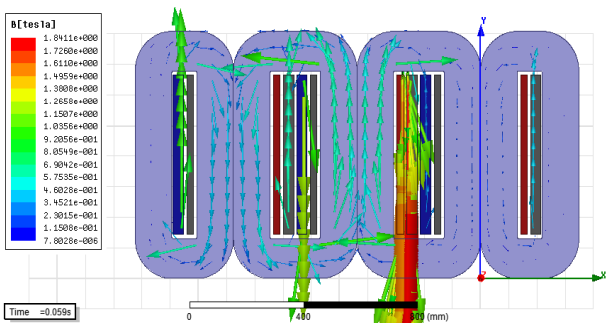

Figure 6. *Magnetic field distribution at max short circuit current with t = 59 ms.*

As seen in figure 6, at t = 59 ms, when the short-circuit current in phase B reaches its peak, the leakage magnetic field in the winding area increases to B=1.84T, while the magnetic field in the core decreases. At this moment, the highest concentration of leakage magnetic flux is observed in the middle of the LV and HV windings.

+ Short-circuit currents of the APCTs of 50 kVA-22/0,4 kV

The APCTs is simulated for three-phase short circuit conditions and analyzed in FEM 3D analysis.

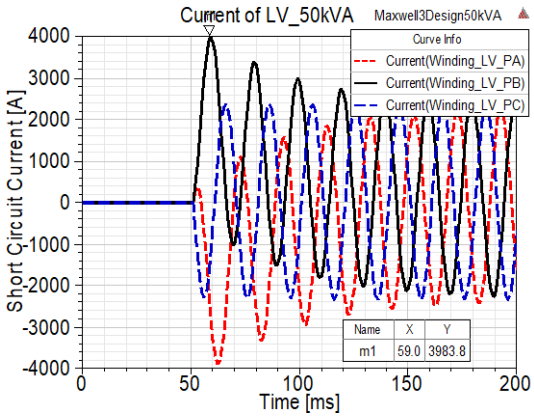

Figure 7. *Short-circuit currents in the LV winding.*

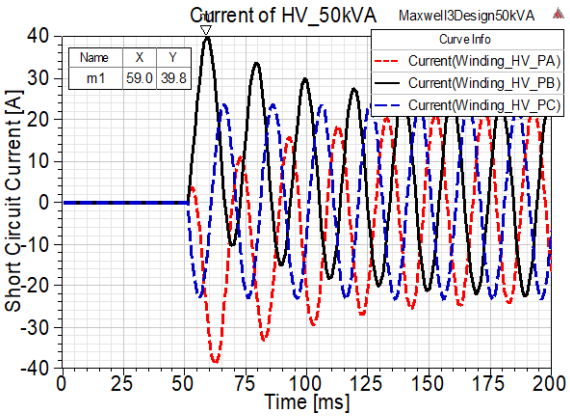

Figure 8. *Short-circuit currents in the HV winding.*

The results of the short-circuit current analysis for the LV and HV windings are shown in figure 7 and figure 8. At t = 59 ms, the maximum short-circuit current amplitudes are: I_{LV_max} = 3983.8 A for the LV winding (phase B) and I_{HV_max} = 39.8 A for the HV winding. These values are up to 39 times greater than the rated current amplitude.

Table 2. *Maximum values in LV and HV windings.*

Windings	**Rated current amplitude (A)**	**Maximum short-circuit current amplitude (A)**		**Error (%)**
		Matlab	**FEM**	
LV winding	$72.17\sqrt{2}$	4007.3	3983.8	0.6
HV winding	$0.76\sqrt{2}$	41.15	39.8	3.3

+ Results of electromagnetic force acting in the HV and LV windings

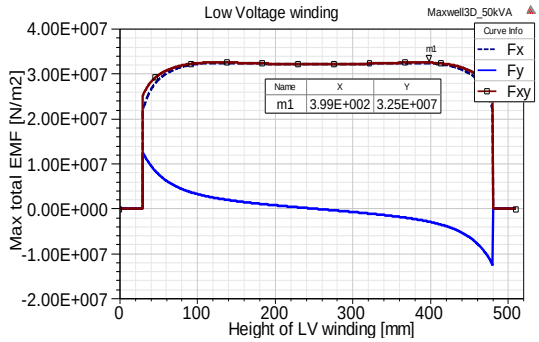

Figure 9. *The maximum total electromagnetic force Fxy of the LV winding.*

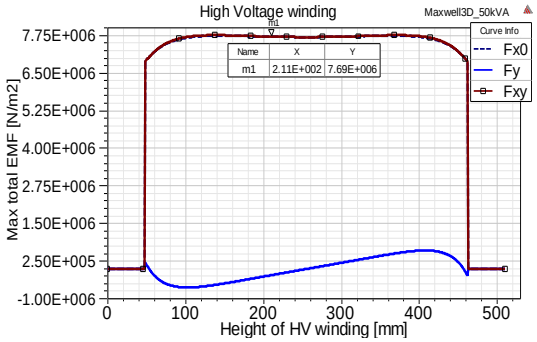

Figure 10. *The maximum total electromagnetic force Fxy of the HV winding.*

The investigation of the EMFs acting on the windings at the Transformer's cross-section on the 0xy plane is presented in figure 6. At this cross-section, the magnetic component Bz (coincident with the current) is 0. Therefore, this applied force is divided into two components:

+ Radial force: $F_{x\_radial} = B_y.J_z$

+ Axial force: $F_{y\_axial} = B_x.J_z$

The total EMFs is defined as: $F_{xy\_total} = \sqrt{F_{x\_radial}^2 + F_{y\_axial}^2}$ (N/m^2)

Figure 9 and figure 10 shows the components of the electromagnetic force acting directly on the LV and HV windings.

It can be seen that the distribution of the F_x in the LV and HV windings has the smallest value at the two ends of the winding. This EMFs increases in the middle of the winding and gets the maximum value at the middle of the winding. However, the distribution of the F_y has the maximum values at the two ends of each winding, and these EMFs become zero in the middle of the windings. The results of EMFs are shown in table 3.

Table 3. *Maximum values of EMFs on LV and HV wingdings.*

Total electromagnetic force F_{xymax} (N/m^2)	**HV winding**	**LV winding**
F_{xymax}	0.769×10^7	3.255×10^7
Allowable stress limit: σ_{ASL}	5.10^7	
Comparing F_{xymax} with σ_{ASL}	$3.255\times10^7 < 5\times10^7$	

In table 3, the largest EMFs is $F_{xymax} = 3.255\times10^7$ N/m^2 while the allowable stress of copper wire $\sigma_{ASL} = 5\times10^7$ N/m^2 [10]. When the short-circuit current value is 39 times larger than the rated current, the maximum EMFs on the windings have not exceeded the allowable limit. Therefore, the structure of the HV and LV windings can not be broken.

4. SIMULATION OF A POWER SERIES OF APCTs

4.1. Resultant EMFs on LV winding for a series of winding radius r

In this section, the paper is analyzed with the change of LV winding radius based on the values of r = 5; 10; 15; 18; 30; 50; 100 mm.

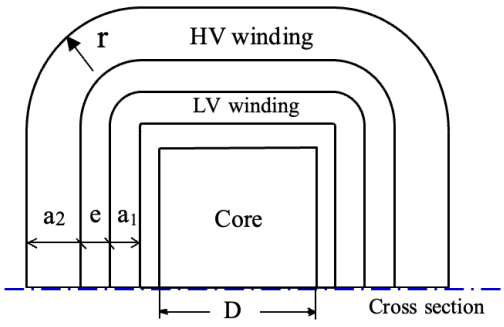

Figure 11. *Radius r of LV and HV windings.*

Table 4. *Total maximum EMFs at r =5; 10; 15; 18; 30; 50 và 100 mm.*

Winding radius (mm)	**Total maximum EMFs (x10^7 N/m^2)**	
	LV	**HV**
5	10.255	6.324
10	9.520	6.206
15	8.789	5.975
18	8.269	5.844
30	7.509	5.552
50	6.522	4.875
100	3.532	4.119

The APCTs is simulated in the LV winding short circuit fault, the paper is analyzed in the time domain with a stop time of 0.1 s and a step time of 0.001 s. The maximum short-circuit EMFs values are then compared and evaluated. The distribution results of EMFs acting on the LV and HV windings corresponding to different radii are shown in figure 12 and figure 13. The results show that the EMFs are the largest at the radius r = 5 mm (the highest value curve). On the contrary, the EMFs value is the smallest at r = 100 mm (the lowest value curve); the EMFs value is evenly distributed on the winding loop. At this time, the winding loop structure is almost circular. The largest EMFs values of the 7 cases of varying radius r are shown in table 4.

In this paper, it needs to show the dependence of the EMFs value based on the winding radius r. The result of the largest EMFs is shown in table 4 and the the EMFs value according to the winding radius r in figure 14. When the winding radius r value increases, the EMFs decreases and

vice versa. The winding radius r value increases from 5 to 100 mm, corresponding to the EMFs on the LV winding decreasing from 10.255×10^7 N/m^2 down to 3.532×10^7 N/m^2.

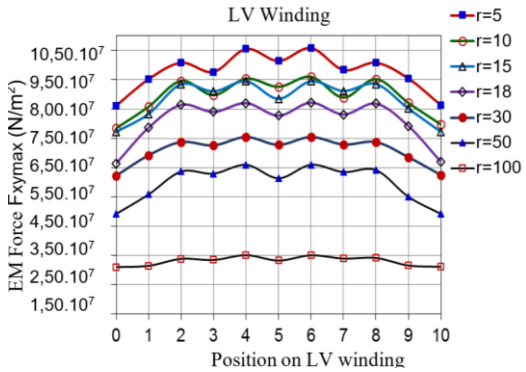

Figure 12. *Distribution of EMFs on LV winding with a series of radius r.*

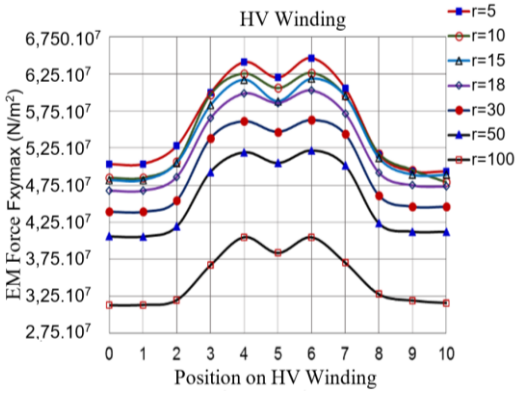

Figure 13. *Distribution of EMFs on HV winding with a series of radius r.*

The increased rate of EMFs when radius r increases from 5 mm to 100 mm, that is:

$$K = \frac{F_{r=5mm}}{F_{r=100mm}} = \frac{10.255}{3.532} = 2.9$$

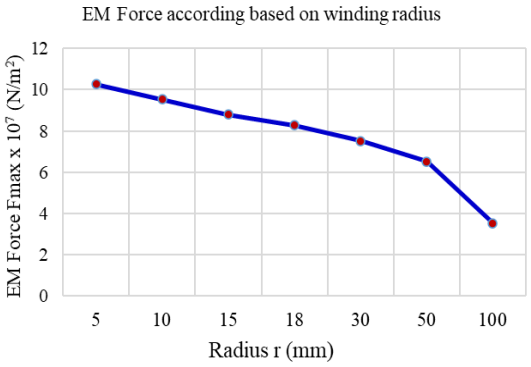

Figure 14. *The EMFs value based on the winding radius r.*

The results show that when the winding radius r is reduced from 100 mm to 5 mm, the increase coefficient of the EMFs acting on the winding is 290%.

4.2. Resultant EMFs on LV and HV winding for a power series of APCTs

The FEM is now used to simulate multiple transformers with different capacities. Simulations are conducted for ten different power-rated APCTs. As shown in table 5, all transformers have a voltage rating of 22/0.4 kV and a Δ/Y winding configuration.

Table 5. *Basic parameters of a three-phase APCTs.*

No	Parameters		Power (kVA)									
			50	***100***	***160***	***250***	***400***	***630***	***750***	***1000***	***1250***	***1600***
1	Winding turns (turns)	HV	4002	3001	2802	2603	2001	1715	1605	1400	1305	1001
		LV	40	30	28	26	20	18	16	14	13	10
2	Phase currents (A)	HV	0.76	1.51	2.42	3.79	6.06	9.55	11.36	15.15	18.94	24.24
		LV	72.17	144.34	231	360.84	577.4	909.33	1082.53	1443.4	1804.22	2309.4
3	No load i_0%		0.8	0.7	0.6	0.55	0.53	0.52	0.51	0.50	0.50	0.50
4	voltage u_k%		4.2	4.3	4.17	4.4	4.4	5.7	5.65	5.6	5.62	5.6

As a result, the EMFs were simulated in LV and HV windings of APCTs with a series of power S = 50 ÷ 1600 kVA. The results of the 10 cases above are shown in table 6.

Table 6. *Basic parameters of a three-phase AMTC.*

Parameter		**Power (kVA)**									
		50	***100***	***160***	***250***	***400***	***630***	***750***	***1000***	***1250***	***1600***
Total EMFs $F_{xymax} \times 10^7$ (N/m^2)	HV winding	0.769	1.248	2.553	2.701	3.102	3.427	4.572	3.544	7.125	15.76
	LV winding	3.255	4.158	7.419	6.077	4.781	5.444	7.620	5.969	11.88	24.10

The characteristic represents the short-circuit EMFs values in LV and HV windings of APCTs with a power series of APCTs S = 50 ÷ 1600 kVA as shown in figure 15.

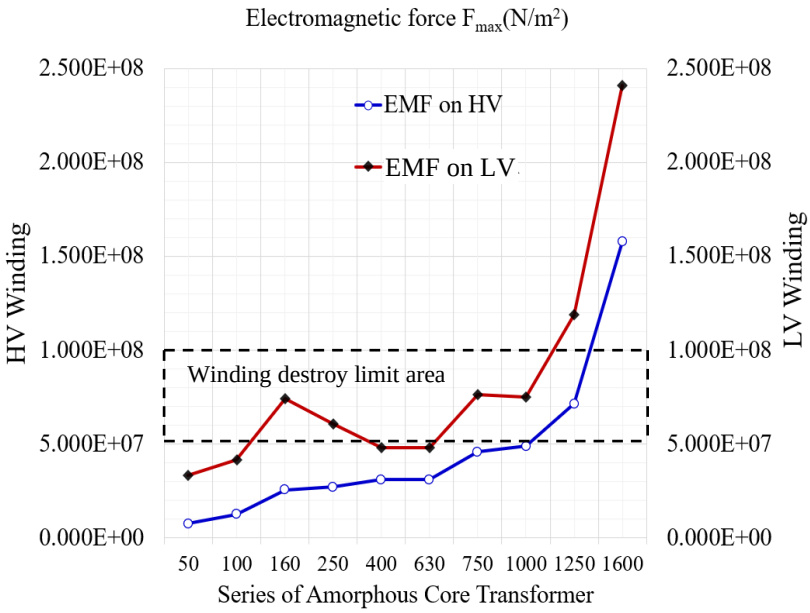

Figure 15*. Characteristics of short-circuit EMFs in windings based on a power series of APCTs.*

* *Discussion:*

+ The maximum short-circuit EMFs value on the LV winding is greater than that of the HV winding, the allowable stress limit of the LV winding needs to be verified. Since the LV winding is situated inside the HV winding, it is influenced by a more diffuse magnetic field, resulting in larger EMFs acting on it.

+ Comparing the EMFs acting on the windings with the winding destruction limit, we observe that as transformer power increases, the design minimizes the mass of steel and copper. Consequently, the ability to withstand short-circuit EMFs diminishes. When a transformer experiences a short-circuit failure, the maximum EMFs in the winding exceed the allowable stress limit of the copper winding.

4.3. Technical guide for a power series of APCTs

The ability of short-circuit EMFs to destroy the winding for a power series of APCTs is divided into 3 areas: Safe area, danger area and destroy area.

1) Technical guide 1 for LV winding: As seen in the characteristics shown in figure 15, the destruction of the LV winding due to short-circuit EMFs is illustrated in figure 16.

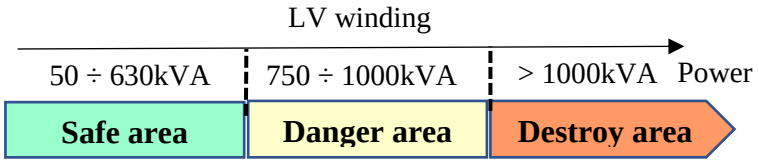

Figure 16. *The allowable EMFs limit of LV winding according to a power series of APCTs.*

2) Technical Guide 2 for HV winding: Similarly, the destruction of the HV winding due to short-circuit EMFs is illustrated in figure 17.

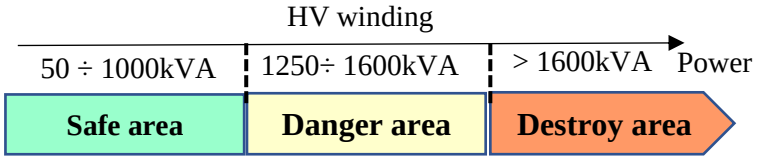

Figure 17. *The allowable EMFs limit of HV winding according to a power series of APCTs.*

**Discussion:* Examining the two figures 16 and 17, we can observe the correlation between APCTs design capacity and the winding's ability to endure destructive forces.

+ In terms of operation: When a short circuit occurs, the higher the capacity, the more susceptible the LV winding is to damage, warping, or even breaking compared to the HV winding.

+ In terms of design: As the transformer capacity increases (especially ≥ 1000 kVA), the LV winding requires reinforcement, more secure positioning, or a larger winding cross-section than the HV winding.

5. CONCLUSIONS

This paper calculates the short-circuit current and analyzes the EMFs components acting on the LV and HV windings of APCTs. The analysis and evaluation were conducted using MATLAB and FEM simulations in Ansys Maxwell 3D, applied to APCTs of 50 kVA – 22/0.4 kV. The results show that the maximum magnetic field and short-circuit current in the LV and HV windings can be up to 39 times the rated current amplitude. **Result 1**: The paper simulates seven cases in Ansys Maxwell 3D with winding curvature radius of r = 5, 10, 15, 18, 30, 50, and 100 mm. The findings establish a relationship between the short-circuit EMFs and the winding curvature radius. The model indicates that a smaller curvature radius (i.e., a nearly rectangular winding) results in the shortest winding length and the lowest copper weight. However, this comes at the cost of higher short-circuit EMFs. **Result 2:** The study extends the simulation to a power range of 50 to 1600 kVA – 22/0.4 kV APCTs. The results define the short-circuit EMFs characteristics on LV and HV windings across different power levels. From this, two technical guidelines are proposed: (1) assessing the permissible EMFs limits on LV and HV windings for various APCTs power ratings and (2) utilizing characteristic curves to evaluate winding stress relative to its strength limit. These insights assist designers, manufacturers, and operators in accurately determining winding conditions under short-circuit EMFs exposure for each APCTs power level.

Future research will focus on two key directions. First, the study will develop electromagnetic force characteristic curves for a wider range of machine power levels. Second, it will optimize the selection of the curvature radius r to minimize winding weight while ensuring the required short-circuit EMFs on the windings.

REFERENCES

[1]. K. Dawood, F. Elieyioğlu and S. Tursun, *"Experimental comparison of weight and cost for MOH and amorphous transformer cores,"* 2024 5th International Conference on Communications, Information, Electronic and Energy Systems (CIEES), Veliko Tarnovo, Bulgaria, pp. 1-4, (2024). DOI: 10.1109/CIEES62939.2024.10811337.

[2]. Z Z. Wang, Z. Shao, S. Niu, B. Jia, X. Chen and X. Dai, *"Study of transformer winding vibration characteristics under electromagnetic field and structural force field,"* 2023 IEEE 4th China International Youth Conference On Electrical Engineering (CIYCEE), Chengdu, China, pp. 1-6, (2023). DOI: 10.1109/CIYCEE59789.2023.10401641.

[3]. L. Roginskaya, Z. Yalalova, A. Gorbunov, and J. Rakhmanova, *"Features of amorphous steel magnetic cores for transformers operating at mains frequency,"* Proc. - ICOECS Int. Conf. Electrotech. Complexes Syst., pp. 12–16, (2020). DOI: 10.1109/ICOECS50468.2020.9278451.

[4]. M. E. M. Nazmunnahar M, S. Simizu, P. R. Ohodnicki and S. Bhattacharya, *"Finite-element analysis modeling of high-frequency single-phase transformers enabled by metal amorphous nanocomposites and calculation of leakage inductance for different winding topologies,"* IEEE Trans. Magn., vol. 55, no. 7, pp. 1–11, (2019). DOI: 10.1109/TMAG.2019.2904007.

[5]. Y. Zhai, R. Zhu, Q. Li, X. Wang, Y. Gu and S. Li, *"Simulation research on electrodynamic force and deformation of transformer windings under short-circuit condition,"* 2022 IEEE International Conference on High Voltage Engineering and Applications (ICHVE), pp. 1-4, (2022). DOI: 10.1109/ICHVE53725.2022.9961358.

[6]. S. Bal, T. Demirdelen and M. Tümay, *"Three-phase distribution transformer modeling and electromagnetic transient analysis using ANSYS Maxwell,"* 2019 3rd International Symposium on Multidisciplinary Studies and Innovative Technologies (ISMSIT), Ankara, Turkey, pp. 1-4, (2019). DOI: 10.1109/ISMSIT.2019.8932953.

[7]. D. C. Phi, D. T. Bao, L. K. Dinh, and N. H. Vu, "*Investigate the frequency effect to the deformation and vibration of amorphous steel core transformers,"* 2023 8th International Scientific Conference on Applying New Technology in Green Buildings (ATiGB), Danang, Vietnam, pp. 136-141, (2023). DOI: 10.1109/ATiGB59969.2023.10364391.

[8]. E. Kaewchinda and M. Thawornphan, *"Improving the efficiency of power distribution systems with distribution transformers amorphous core type,"* 2023 IEEE PES 15th Asia-Pacific Power and Energy Engineering Conference (APPEEC), Chiang Mai, Thailand, pp. 1-4, (2023). DOI: 10.1109/APPEEC57400.2023.10562014.

[9]. A. C. De Azevedo, A. C. Delaiba, J. C. De Oliveira, B. C. Carvalho, and H. D. S. Bronzeado, *"Transformer mechanical stress caused by external short-circuit : a time domain approach,"* Present. Int. Conf. Power Syst. Transients, in Lyon, France, June 4-7, pp. 1–6, (2007).

[10]. H. Ahn, J. Lee, J. Kim, Y. Oh, and S. Jung, *"Finite-element analysis of short-circuit electromagnetic force in power transformer,"* IEEE Trans. Ind. Appl., vol. 47, no. 3, pp. 1267–1272, (2011). DOI: 10.1109/TIA.2011.2126031.

[11]. H. Ahn, Y. Oh, J. Kim, J. Song, and S. Hahn, *"Experimental verification and finite element analysis of short-circuit electromagnetic force for dry-type transformer,"* IEEE Transactions on Magnetics, vol. 48, no. 2, pp. 819–822, (2012).

[12]. D. T. Bao D. C. Phi, H. D. Hoan and L. T. Hiep, *"Analysis of current and electromagnetic force acting on winding in cases of short circuits of amorphous transformer,"* Appl. New Technol. Green Build. ATiGB 2023, pp. 201–208, (2023). DOI: 10.1109/ATiGB59969.2023.10364484.

[13]. Y. Song, Y. Lu, L. Zhang *et al.*, *"Electromagnetic force analysis of short-circuit faults in transformer windings based on fractional-order models,"* 2024 3rd Asian Conference on Frontiers of Power and Energy (ACFPE), Chengdu, China, pp. 514-520, (2024). DOI: 10.1109/ACFPE63443.2024.10800964.

[14]. K. Dawood, S. Tursun and G. Kömürgöz, *"Optimized gap positions for improved electromagnetic forces in dry-type transformer design,"* 2024 6th Global Power, Energy and Communication Conference (GPECOM), Budapest, Hungary, pp. 211-215, (2024). DOI: 10.1109/GPECOM61896.2024.10582721.

[15]. Y. Yu, Z. Zhanlong, H. Wenhao, C. Junxin and L. Dingyuan, *"Simulation analysis of inrush current and electromagnetic-force characteristics of converter transformer during no-load closing,"* 2023 2nd International Conference on Power Systems and Electrical Technology (PSET), Milan, Italy, pp. 137-143, (2023). DOI: 10.1109/PSET59452.2023.10346443.

[16]. Q. Wang, L. Wang, Z. Yuan *et al.*, *"Analysis of three-phase short-circuit electrodynamic variation characteristics of power transformers,"* 2023 7th International Conference on Electrical, Mechanical and Computer Engineering (ICEMCE), Xi'an, China, pp. 397-400, (2023). DOI: 10.1109/ICEMCE60359.2023.10490632.

[17]. Y. Jing, C. Chen, Y. Liu, Z. Yu and Y. Li, *"Analysis of winding forces in transformer under no-load closing condition based on field-circuit coupling method,"* 2023 IEEE International Conference on Applied Superconductivity and Electromagnetic Devices (ASEMD), Tianjin, China, pp. 1-2, (2023). DOI: 10.1109/ASEMD59061.2023.10369219.

[18]. Y. Zhao, T. Wen, Y. Li, H. Ni, Q. Zhang and W. Chen, *"A FEM-based simulation of electromagnetic forces on transformer windings under short-circuit,"* 2018 IEEE International Power Modulator and High Voltage Conference (IPMHVC), Jackson, WY, USA, pp. 425-429, (2018). DOI: 10.1109/IPMHVC.2018.8936726.

[19]. Q. Z. Mingkai Jin, T. Wen, W. Chen *et al.*, "*Influence of frequency components of short-circuit electromagnetic force on vibration characteristics of power transformer windings*," 2022 IEEE International Conference on High Voltage Engineering and Applications (ICHVE), Chongqing, China, pp. 01-04, (2022). DOI: 10.1109/ICHVE53725.2022.9961671.

[20]. K. Dawood and G. Komurgoz, *"Investigating effect of electromagnetic force on sandwich winding transformer using finite element analysis,"* 2021 28th Int. Work. Electr. Drives Improv. Reliab. Electr. Drives, IWED 2021 - Proc., pp. 1–5, (2021). DOI: 10.1109/IWED52055.2021.9376371.

[21]. C. Zhao, W. Chen, M. Jin, T. Wen *et al.*, *"Short-circuit electromagnetic force distribution characteristics in transformer winding transposition structures,"* IEEE Trans. Magn., vol. 56, no. 12, pp. 1–8, (2020). DOI: 10.1109/TMAG.2020.3028832.

[22]. D. T. Bao and D. C. Phi, *"Calculation of the magnetic field and inrush current in a three-phase transformer,"* Proc. 2020 Appl. New Technol. Green Build. ATiGB 2020, pp. 94–99, (2020). DOI: 10.1109/ATiGB50996.2021.9423111.

TÓM TẮT

Xác định vùng giới hạn phá hủy cuộn dây của dãy công suất của máy biến áp lõi vô định hình

Máy biến áp lõi thép vô định hình có cấu trúc đặc biệt của lõi thép và cuộn dây là hình chữ nhật nên phân bố lực điện từ lên dây quấn không đồng đều như cuộn dây hình tròn của máy lõi silic. Do đó, việc đánh giá các giá trị gia tăng lực điện từ và xác định khu vực phá huỷ của dây quấn là rất cần thiết. Bài báo đã sử dụng phần mềm Matlab và FEM bằng Ansys Maxwell 3D để tính toán từ trường, dòng điện ngắn mạch, lực điện từ của dãy công suất máy biến áp vô định hình 3 pha điện áp 22/0,4 kV khi bị sự cố ngắn mạch. Kết quả của bài báo, xây dựng mối quan hệ giữa giá trị lực điện từ ngắn mạch với bán kính dây quấn; và xác định khu vực giới hạn phá huỷ cuộn dây theo dãy công suất máy biến áp. Dựa vào các kết quả nghiên cứu này, giúp nhà thiết kế, chế tạo và nhà vận hành máy biến áp, xác định đúng tình trạng của dây quấn khi bị tác động của lực điện động ngắn mạch gây ra.

Từ khóa: Máy biến áp; Vô định hình; Lực điện từ; Từ trường; Ngắn mạch.